Exploring organ-specific features of fibrogenesis using murine precision-cut tissue slices

Bigaeva, Emilia; Gore, Emilia; Mutsaers, Henricus A M; Oosterhuis, Dorenda; Kim, Yong Ook; Schuppan, Detlef; Bank, Ruud A; Boersema, Miriam; Olinga, Peter

Published in:
Biochimica et biophysica acta-Molecular basis of disease

DOI:
10.1016/j.bbadis.2019.165582

Publication date:
2020

BBA - Molecular Basis of Disease 1866 (2020) 165582

Contents lists available at ScienceDirect

BBA - Molecular Basis of Disease

journal homepage: www.elsevier.com/locate/bbadis

Exploring organ-specific features of fibrogenesis using murine precision-cut tissue slices

Emilia Bigaeva[a], Emilia Gore[a], Henricus A.M. Mutsaers[a,b], Dorenda Oosterhuis[a], Yong Ook Kim[c], Detlef Schuppan[c,d], Ruud A. Bank[e], Miriam Boersema[a], Peter Olinga[a,*]

[a] Department of Pharmaceutical Technology and Biopharmacy, University of Groningen, the Netherlands
[b] Department of Clinical Medicine, Aarhus University, Denmark
[c] Institute of Translational Immunology and Research Center for Immunotherapy, University Medical Center, Johannes Gutenberg University, Obere Zahlbacherstraße 63, Mainz 55131, Germany
[d] Division of Gastroenterology, Beth Israel Deaconess Medical Center, Harvard Medical School, Boston, 330 Brookline Avenue, MA 02215, USA
[e] Department of Pathology and Medical Biology, University of Groningen, University Medical Center Groningen, the Netherlands

ARTICLE INFO

Keywords:
Precision-cut tissue slices
Fibrosis
TGFβ
Extracellular matrix
Collagen
SMAD2

ABSTRACT

Fibrosis is the hallmark of pathologic tissue remodelling in most chronic diseases. Despite advances in our understanding of the mechanisms of fibrosis, it remains uncured. Fibrogenic processes share conserved core cellular and molecular pathways across organs. In this study, we aimed to elucidate shared and organ-specific features of fibrosis using murine precision-cut tissue slices (PCTS) prepared from small intestine, liver and kidneys. PCTS displayed substantial differences in their baseline gene expression profiles: 70% of the extracellular matrix (ECM)-related genes were differentially expressed across the organs. Culture for 48 h induced significant changes in ECM regulation and triggered the onset of fibrogenesis in all PCTS in organ-specific manner. TGFβ signalling was activated during 48 h culture in all PCTS. However, the degree of its involvement varied: both canonical and non-canonical TGFβ pathways were activated in liver and kidney slices, while only canonical, Smad-dependent, cascade was involved in intestinal slices. The treatment with galunisertib blocked the TGFβRI/SMAD2 signalling in all PCTS, but attenuated culture-induced dysregulation of ECM homeostasis and mitigated the onset of fibrogenesis with organ-specificity. In conclusion, regardless the many common features in pathophysiology of organ fibrosis, PCTS displayed diversity in culture-induced responses and in response to the treatment with TGFβRI kinase inhibitor galunisertib, even though it targets a core fibrosis pathway. A clear understanding of the common and organ-specific features of fibrosis is the basis for developing novel antifibrotic therapies.

1. Introduction

Excessive scar formation, known as fibrosis, is a common pathological factor in numerous chronic diseases affecting various organs such as the liver, kidneys, intestine, lungs and skin, among others. Pathologies like Crohn's disease, primary biliary cholangitis and chronic kidney disease cause progressive organ malfunction, resulting in high morbidity and mortality [1–3]. Despite the fact that diverse factors can cause aberrant wound healing, the pathogenesis of fibrosis shares a number of common features across organs [4,5]. Under chronic injury, fibroblasts differentiate into myofibroblasts – contractile, alpha smooth muscle actin (α-SMA) positive cells – that secrete excessive amounts of extracellular matrix (ECM) proteins and glycoproteins, such as collagen, fibronectin, elastin, biglycan and decorin [6]. ECM remodelling is regulated by matrix metalloproteinases (MMPs) that degrade ECM, and their inhibitors – tissue inhibitors of metalloproteinases (TIMPs). Fibrosis occurs when the balance between MMPs and TIMPs shifts towards the latter, meaning that the synthesis of new ECM by myofibroblasts exceeds the rate at which it is degraded [7]. Other shared characteristics of fibrosis include the release of pro-fibrogenic cytokines and growth factors, impaired angiogenesis [8] and sustained inflammation [9,10].

Furthermore, fibrosis-associated signalling pathways are highly conserved between different organs. For instance, transforming growth factor beta (TGFβ) is widely recognized as the key driving force behind fibrogenesis in essentially all organs [11–15]. Excessive release and

* Corresponding author at: University of Groningen, Department of Pharmaceutical Technology and Biopharmacy, Antonius Deusinglaan 1, 9713 AV Groningen, the Netherlands.
E-mail address: p.olinga@rug.nl (P. Olinga).

https://doi.org/10.1016/j.bbadis.2019.165582
Received 16 May 2019; Received in revised form 6 October 2019; Accepted 16 October 2019
Available online 30 October 2019

sustained activity of TGFβ stimulates cellular differentiation to myofibroblasts and pathological ECM turnover [4]. The TGFβ signalling cascade involves the binding of a ligand to the extracellular domain of the type II receptor (TGFβRII) that recruits and phosphorylates the type I receptor (TGFβRI or activin receptor-like kinase 5, ALK5). The activated receptor complex triggers the recruitment of SMAD proteins (SMAD2 and SMAD3) that associate with SMAD4 to propagate the signal [16]. Although TGFβ mainly signals *via* SMADs, it can also activate other, non-canonical pathways such as phosphatidylinositol-3-kinase (PI3K)/AKT, Rho-like guanosine triphosphatases (GTPases) and mitogen activated protein kinases (MAPKs), including extracellular signal-regulated kinase (ERK), p38 and c-Jun N-terminal kinase (JNK) [17,18].

Among the available tools to study organ fibrosis, the precision-cut tissue slices (PCTS) model offers several valuable advantages. Opposed to conventional *in vitro* systems, PCTS preserve complex organotypic architecture and retain cell-cell and cell-matrix contacts [19]. Furthermore, PCTS substantially contribute to the 3Rs by reducing the number of animals needed for research, since slices can be prepared from various tissues, enabling simultaneous use of several organs from one animal. Our group previously demonstrated that PCTS can be used to study the mechanisms of intestinal fibrosis [20], liver fibrosis [21,22], renal fibrosis [23,24] and to test the efficacy of putative antifibrotic drugs.

The aim of this study was to uncover the shared and organ-specific features of fibrogenesis in the intestine, liver and kidney using murine PCTS. We explored ECM regulation and involvement of the TGFβ pathway both on a transcriptional and translational level, and investigated organ-specific responses to the treatment with antifibrotic compound galunisertib. Galunisertib (LY2157299 monohydrate) is a small molecule inhibitor of TGFβRI/ALK5 kinase that specifically downregulates the phosphorylation of SMAD2, and it is currently under clinical development for the treatment of a variety of cancers [25–27]. This study improves our general understanding of organ fibrosis for the purposes of basic research and the development of new therapies.

2. Methods

2.1. Animals

Adult C57BL/6J mice (Centrale Dienst Proefdieren, University Medical Center Groningen, Groningen, The Netherlands) were housed under controlled conditions with a 12 h:12 h light-dark cycle and free access to water and food. The experiments were approved by the Animal Ethical Committee of the University of Groningen (DEC 6416AA-001).

Organs were harvested *via* a terminal procedure performed under isoflurane/O_2 anesthesia (Nicholas Piramal, London, UK). Freshly excised livers and kidneys were kept in ice-cold University of Wisconsin (UW) organ preservation solution until slicing. Mouse jejunum was preserved in ice-cold Krebs-Henseleit buffer (KHB) supplemented with 25 mM D-glucose (Merck, Darmstadt, Germany), 25 mM $NaHCO_3$ (Merck) 10 mM HEPES (MP Biomedicals, France), saturated with carbogen (95% O_2/5% CO_2), pH 7.4.

2.2. Preparation of precision-cut tissue slices

Liver, kidney and intestinal PCTS were prepared using a Krumdieck tissue slicer (Alabama Research & Development Corp., Munford, AL, USA) according to the protocol described by de Graaf et al. [28] and Stribos et al. [24], with minor modifications.

2.2.1. Precision-cut liver slices (PCLS)

Liver tissue cores were made using a 6 mm biopsy punch. Slices with a wet weight of 4–5 mg and estimated thickness of 250–300 μm were prepared in ice-cold KHB and transferred to UW directly after slicing, to prevent rapid loss of viability. Slices were incubated individually in 1.3 mL of Williams' medium E with GlutaMAX (Life Technologies, Bleiswijk, the Netherlands) supplemented with 25 mM D-glucose (Merck) and 50 μg/mL gentamicin (Life Technologies) at 37 °C in an 80% O_2/5% CO_2 atmosphere while gently shaken at 90 rpm.

2.2.2. Precision-cut kidney slices (PCKS)

Whole mouse kidneys were placed in the core holder inside the tissue slicer to obtain slices with a wet weight of 4–5 mg and thickness of 250–300 μm. Kidney slices were immediately transferred to ice-cold UW after slicing. Subsequently, PCKS were incubated individually in 1.3 mL of Williams' medium E with GlutaMAX containing 10 μg/mL ciprofloxacin (Sigma-Aldrich, Saint Louis, USA) and 25 mM D-glucose (Sigma-Aldrich) at 37 °C in a 80% O_2/5% CO_2 atmosphere while gently shaken at 90 rpm.

2.2.3. Precision-cut intestinal slices (PCIS)

The jejunum was cleaned by flushing KHB through the lumen, the tissue was subsequently divided into 2 cm segments. These segments were filled with 3% (*w/v*) agarose (Sigma-Aldrich) in 0.9% NaCl at 37 °C and embedded in an agarose core-embedding unit. Intestinal slices with wet weight of 1–2 mg were prepared and stored in ice-cold KHB, then cultured individually in 0.5 mL of Williams' medium E with GlutaMAX supplemented with 25 mM D-glucose, 50 μg/mL gentamicin and 2.5 μg/mL fungizone (amphotericin B; Life Technologies) at 37 °C in an 80% O_2/5% CO_2 atmosphere while gently shaken at 90 rpm.

2.3. Experimental treatment of PCTS with galunisertib (LY2157299)

Galunisertib (LY2157299) was purchased from Selleckhem (Munich, Germany). Stock solution of 2.5 mM was prepared in DMSO and diluted in the culture medium with a final concentration of the solvent of ≤0.5%. Mouse liver, kidney and intestinal slices were incubated with 10 μM of galunisertib or solvent for 48 h. The tested concentration of galunisertib was in the range of observed plasma exposure [29,30]. Medium was refreshed every 24 h.

2.4. Viability of PCTS

After incubation, slices were transferred to a sonication solution (containing 70% ethanol and 2 mM EDTA) and snap-frozen [28]. Viability of the slices was assessed by measuring the adenosine triphosphate (ATP) content using the ATP bioluminescence kit (Roche diagnostics, Manheim, Germany). The ATP values (pmol) were normalized to the total protein content (μg) of each slice, estimated by the Lowry assay (Bio-Rad DC Protein Assay, Hercules, USA). Values are displayed as relative values compared to the average of a related control.

2.5. Total RNA isolation cDNA synthesis

Total RNA was isolated from pooled snap-frozen slices (three slices for liver and kidney, six slices for jejunum), using the Qiagen RNAeasy mini kit (Qiagen, Venlo, The Netherlands). The absorbance ratio 260/280 was used to assess RNA purity and was considered satisfactory when values ranged between 1.9 and 2.1. Reverse transcription was performed with 1 μg total RNA using the Reverse Transcription System (Promega, Leiden, The Netherlands) at 25 °C for 10 min, 42 °C for 15 min and 95 °C for 5 min.

2.6. Mouse TaqMan low-density array

We used a custom-designed Taqman low-density array (TLDA, Applied Biosystems, Bleiswijk, The Netherlands) to measure the expression of 44 genes related to extracellular matrix homeostasis (Supplementary Table S1). A total of 100 μL reaction mixture containing 6 ng/μL cDNA and 50 μL Taqman Universal PCR Master Mix

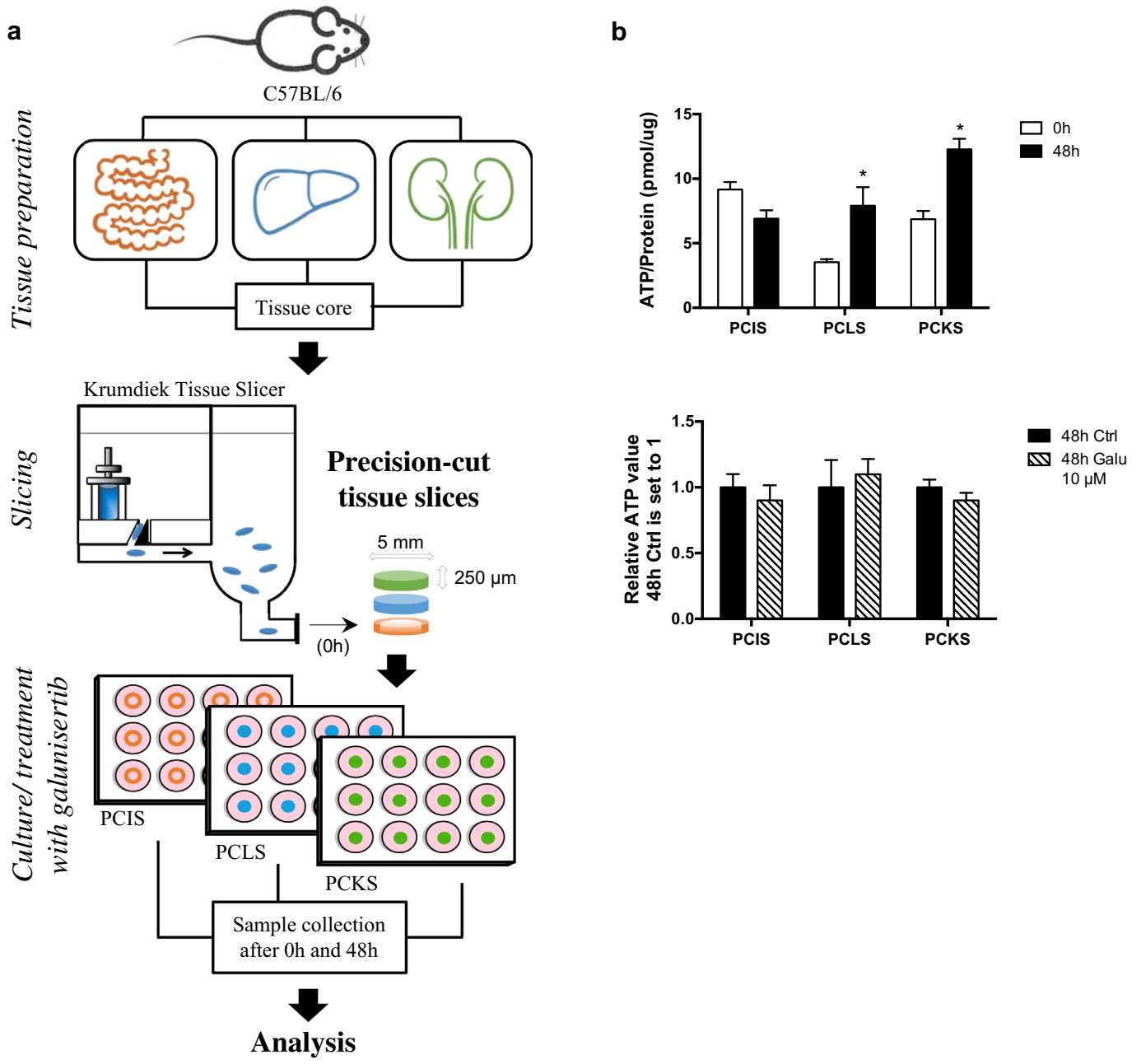

Fig. 1. Preparation, culture and viability of murine precision-cut tissue slices. (a) Graphical summary of the study workflow: precision-cut tissue slices were obtained from murine small intestine (jejunum), liver and kidney by preparing tissue cores that were placed in the Krumdiek tissue slicer. After slicing, PCIS, PCLS and PCKS were cultured in plastic well-plates (1 slice per well) in the presence or absence of galunisertib for 48 h, then collected (by pooling 3–6 slices of the same tissue type and animal from at least three individual mice) and subjected to the analysis. (b) Viability of murine PCIS, PCLS and PCKS at 48 h and after the treatment with 10 µM galunisertib was measured by ATP (pmol) normalized to the total protein content (µg). Data are shown as absolute values to reflect the effect of culture or as relative values to non-treated control slices to reflect the effect of galunisertib. Data are expressed as mean (± SEM), n = 3, *p < 0.05.

(Applied Biosystems) was transferred into the loading port of a TLDA card. PCR amplification was performed on the Applied Biosystems ViiA™7 Real-Time PCR System. The most appropriate housekeeping gene was identified by NormFinder [31]. Based on these results, *Gapdh* was used as an endogenous control. Expression values were calculated using the $2^{-\Delta Ct}$ method [32]. All Ct values above 37 were considered noise and excluded from further analysis. Normalization of the Ct values in each sample was carried out as ΔCt = Ct(target)–Ct(*Gapdh*). The fold change was calculated comparing the gene expression of each group with the average of the control expression level: fold change (FC) = $2^{-\Delta Ct(experimental)}$/mean($2^{-\Delta Ct(control)}$). Gene expression levels were determined relative to 0 h PCIS for baseline expression profiling or to 0 h of respective PCTS for culture and treatment effects. Variance stabilization was managed with $\log_2$ transformation. The heatmap of $\log_2$(FC) values was generated using the online tool Morpheus (https://software.broadinstitute.org/morpheus/). Hierarchical cluster analysis was performed by average-linkage clustering method using Pearson correlation.

2.7. Quantitative real-time PCR

mRNA expression of key fibrosis markers and genes involved in TGFβ signalling was determined with qRT-PCR. The RT-PCR reaction was performed using the SensiMix SYBR Hi-ROX kit (Bioline,

Luckenwalde, Germany) on a 7900HT Real Time PCR system (Applied Biosystems) with a cycle at 95 °C for 10 min and 45 cycles of 95 °C for 15 s and 60 °C for 25 s followed by a dissociation stage. The mRNA expression values were calculated using the $2^{-\Delta Ct}$ method, with *Gapdh* as a reference gene. The primers (50 μM; Sigma-Aldrich) used in this study are listed in Supplementary Table S2.

2.8. Western blotting

Three (for liver and kidney) or six (for jejunum) slices were pooled and lysed in ice-cold RIPA buffer (Thermo Scientific, Waltham, Massachusetts, USA) supplemented with PhosphoStop (Roche Diagnostics, Mannheim, Germany) and protease inhibitor cocktail (Sigma-Aldrich). A total of 90–100 μg of protein was separated by SDS/PAGE on 10% sodium dodecylsulfate polyacrylamide gel, containing 2,2,2-trichloroethanol (TCE; Sigma-Aldrich) for visible detection of total protein load [33], and subsequently transferred to an activated polyvinyl difluoride membrane (Immuno-Blot PVDF, Bio-Rad). Membranes were blocked in TBST with 5% Blotting-Grade Blocker (Bio-Rad) and incubated with primary antibody (Supplementary Table S3) overnight at 4 °C. Immunodetection was performed by incubating the membranes with the appropriate HRP-conjugated secondary antibody. Protein bands were visualized using Clarity Western ECL Substrate (Bio-Rad) and ChemiDoc Touch Imaging System (Bio-Rad). Protein expression was corrected for total protein load and expressed as a relative value to the control group.

2.9. Statistics

The aforementioned analyses were performed using three to six pooled slices from the same animal (technical replicates) and repeated with at least three mice (biological replicates). The results are expressed as mean ± standard error of mean (SEM). We used GraphPad Prism 6.0 (GraphPad Software Inc.) to carry out statistical data analysis. Treatment groups were compared by unpaired Student's *t*-test or one-way ANOVA followed by Dunnett's multiple comparisons test as appropriate. Protein levels determined by Western blot were compared using non-parametric Mann-Whitney test. A p-value of < 0.05 was considered statistically significant.

3. Results

We used murine small intestine (jejunum), liver and kidney to prepare precision-cut tissue slices (PCIS, PCLS and PCKS, respectively) as illustrated in Fig. 1a. Slices were cultured for 48 h under standard conditions or treated with TGFβR1 kinase inhibitor galunisertib. Fig. 1b shows that all slices remained viable at 48 h, in accordance with our previous reports [24,34]. PCIS displayed a slight decrease in ATP content, while the ATP levels of PCLS and PCKS significantly increased at 48 h, indicating that ATP production was restored after the cold ischemia period as a result of slicing. In line with previous reports [22], galunisertib at 10 μM did not elicit toxicity in PCIS, PCLS or PCKS, as it had no impact on ATP content.

3.1. Differential regulation of genes involved in ECM homeostasis in PCTS

To characterize the regulation of ECM homeostasis, we carried out gene expression profiling of tissue slices at 0 h, after 48 h of culture or after the treatment with a TGFβR1 kinase inhibitor galunisertib. We performed TaqMan low density array (TLDA) with a panel of 44 genes related to various ECM components (including six types of collagen), enzymes involved in collagen processing and ECM remodelling and ECM protein receptors.

Fig. 2a illustrates the baseline ECM (regulation) expression profiles of PCIS, PCLS and PCKS, as visualized by a heatmap with hierarchical clustering. Unsupervised cluster analysis of relative expression levels ($\log_2$(FC) values) provided a perfect separation of 0 h PCIS, PCLS and PCKS, suggesting substantial differences in the baseline ECM regulation profiles between intestine, liver and kidney. A comparative statistical analysis revealed that only 13 out of 44 transcripts (30%) had similar expression levels in all PCTS (Supplementary Table S4). Furthermore, we identified seven genes (*Plod2*, *Leprel1*, *Loxl2*, *Mmp13*, *Bmp1*, *Fn1* and *Ddr2*) that were differentially expressed across all PCTS (Fig. 2b). Fig. 2c–e illustrates the sets of transcripts that represent distinct signatures in PCTS baseline expression profiles. For instance, PCIS at 0 h highly expressed genes encoding collagens (*Col1a1*, *Col3a1*, *Col6a1*) and metalloproteinases (*Mmp2* and *Mmp9*). PCLS, in turn, exhibited characteristically low expression of five transcripts (*Col1a2*, *Col4a1*, *Loxl1*, *Serpinh1* and *Ddr1*), while PCKS expressed high levels of other six mRNAs (*Leprel2*, *Pcolce*, *Slc39a13*, *Fmod*, *Bgn* and *Mrc2*) and low levels of *P4hb* and *Dcn*.

We next examined the impact of 48 h culture and the treatment with TGFβRI kinase inhibitor (Fig. 3). Both culture and galunisertib introduced considerable changes in the gene expression profiles of PCIS, PCLS and PCKS, as the cluster analysis clearly separated the samples by time point (0 h *vs.* 48 h) and treatment (48 h control slices *vs.* 48 h slices treated with 10 μM galunisertib) (Fig. 3a–c). The effect of culture in PCTS is summarized in Fig. 3d and f, and Fig. 3e, g and h detail the effect of galunisertib. We performed a pairwise comparison of expression levels in slices at 0 h *versus* 48 h and identified 21 (48%), 26 (59%) and 38 (86%) differentially expressed genes that achieved statistical significance in PCIS, PCLS and PCKS, respectively (Fig. 3d). The majority of these transcripts were upregulated in PCLS (92%) and PCKS (89%), whereas in PCIS 10 out of 21 differentially expressed genes (48%) were downregulated during 48 h culture (Fig. 3d), including *Col1a1*, *Col1a2*, *Col3a1*, *Pcolce*, *Pcolce2*, *Eln* and *Bgn*. The Venn diagram (Fig. 3f) illustrates the numbers of overlapping and unique genes influenced by 48 h culture between PCIS, PCLS and PCKS, followed by the gene lists. Only nine (20%) transcripts were common in all tissue slices: besides altered expression of *Col1a1*, *Col1a2* and *Col3a1*, the organs showed similar culture-induced increase in *P4ha2*, *Lepre1*, *Loxl2*, *Fkbp10*, *Mmp13* and *Timp1*. Furthermore, the number of genes that were shared across pairs of organs dominated over those that were unique within each organ. In particular, PCLS and PCKS exhibited more similar changes in ECM homeostasis at 48 h than their pairwise comparisons with PCIS, as 13 transcripts were commonly affected in PCLS and PCKS, eight transcripts were common between PCIS and PCKS and only three between PCIS and PCLS. As the largest number of differentially expressed genes was observed in cultured PCKS, eight of these genes were unique to PCKS and included *Col6a1*, *Bmp1*, *P4ha1* (required for proper collagen folding), *Loxl3* (involved in crosslinking of collagen and elastin), *Adamts2* and *Adamts3* that are crucial for collagen fibrils formation, and the ECM protein receptors *Ddr2* and *Mrc2*. The top two differentially regulated genes at 48 h in PCIS and PCLS were *Mmp13* (fold change 88.29 ± 23.78 in PCIS, 85.96 ± 7.77 in PCLS) and *Timp1* (fold change 73.21 ± 8.76 in PCIS, 57.89 ± 16.54 in PCLS), while PCKS showed the most dramatic increase in *Mmp9* (fold change 114.34 ± 49.87) and *Timp1* (fold change 684.29 ± 86.05) (Supplementary Table S5). Overall, the culture-induced changes in ECM homeostasis indicate the onset of fibrogenesis in PCTS.

When PCTS were treated with 10 μM galunisertib for 48 h, the degree of the response varied between the organs (Fig. 3e). PCKS displayed an altered expression of 29 genes (66%) with statistical significance. The number of genes affected by galunisertib lowered to nine (20%) in PCLS, and only five genes (11%) were significantly affected in PCIS. Notably, the majority of these transcripts were downregulated; however, some genes were upregulated by galunisertib treatment: *Plod3* (fold change 1.37 ± 0.09 in PCIS), *Loxl4* (fold change 1.29 ± 0.12 in PCLS and 1.41 ± 0.14 in PCKS) and *Dcn* (fold change 3.34 ± 0.12 in PCKS; Supplementary Table S5). Furthermore, statistical analysis revealed that galunisertib significantly downregulated a total of three transcripts across all tissue slices, namely *Lox*, *Col1a1* and

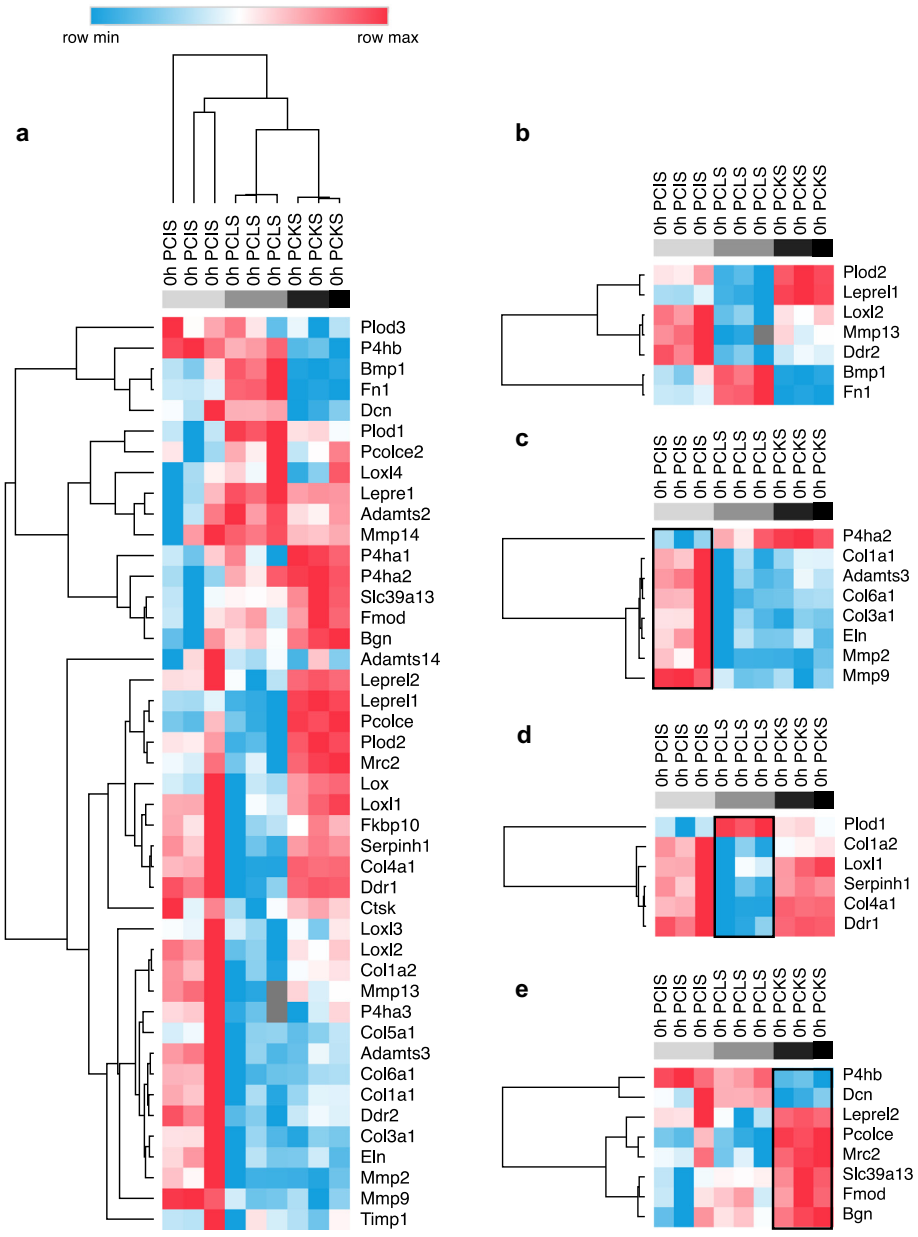

Fig. 2. Transcriptional analysis of murine precision-cut tissue slices prior culturing (0 h) by TaqMan low-density array (TLDA). (a) Heatmap of the expression patterns of 44 genes associated with extracellular matrix homeostasis in 0 h PCIS, 0 h PCLS and 0 h PCKS. The expression levels were calculated as relative to the average expression in 0 h PCIS. Based on statistical analyses performed on ΔCt values (Supplementary Table S4), the transcripts were divided in sets and depicted as portions of the (a) heatmap in the following manner: (b) heatmap illustrating seven genes that were differentially expressed in PCIS, PCLS and PCKS at 0 h; (c) heatmap illustrating genes that are distinct in 0 h PCIS; (d) heatmap illustrating genes that are distinct in 0 h PCLS; (e) heatmap illustrating genes that are distinct in 0 h PCKS. Red and blue indicate relatively high and low expression, respectively (grey color indicates undetermined values). Row min and max expression levels were determined for each row separately, therefore min and max values are unique for each analyzed gene. Unsupervised clustering analysis was performed by average-linkage clustering method using Pearson correlation; n = 3. Full gene names are listed in Supplementary Table S1, and absolute expression values for each gene in PCIS, PCLS and PCKS at 0 h are indicated in Supplementary Table S4.

Col3a1 (Fig. 3g), and the level of downregulation was increasing in the order PCIS < PCLS < PCKS. For instance, galunisertib inhibited *Col1a1* expression by 48% in PCIS, 87% in PCLS and by 97% in PCKS (Supplementary Table S5). Of the 44 tested genes, 13 genes remained unaffected in PCTS after treatment (Fig. 3h) and included genes encoding prolyl hydroxylases *P4ha1*, *P4ha2* and *P4hb*, procollagen N-proteinases *Adamts3* and *Adamts14*, *Col4a1* and ECM protein receptors *Ddr1* and *Ddr2*, among others.

3.2. Regulation of selected markers of fibrogenesis in murine PCTS

To confirm the results of the TLDA, we performed single-gene SYBR green RT-qPCR for selected transcripts. Fig. 4a shows the mRNA level of genes encoding for collagen type I (*Col1a1*), heat shock protein 47 (*Serpinh1*) and fibronectin (*Fn1*) in tissue slices at 0 h, after 48 h culture and after treatment with 10 μM galunisertib. We also included a fourth marker of fibrogenesis — *Acta2*, encoding α-SMA that is expressed by myofibroblasts. The baseline expression of *Col1a1*, *Acta2* and *Fn1* was distinctly higher in PCIS as compared to liver and kidney slices, while *Serpinh1* mRNA level was the lowest in PCLS. All tissue slices developed a spontaneous fibrogenic response during 48 h culture. We observed a significant upregulation of *Serpinh1* and *Fn1* in all organs, upregulation of *Col1a1* and no change in *Acta2* expression in PCLS and PCKS. Of note, the magnitude of culture-induced upregulation varied in an organ-specific manner: the expression level of fibrogenesis markers after 48 h culture were consistently and significantly higher in PCKS than in other tissue slices. In contrast to liver and kidney, PCIS displayed a significant decrease in mRNA levels of *Col1a1* and *Acta2* at 48 h. Overall, our qPCR results for *Col1a1* and *Serpinh1* correlated with TLDA, but not for *Fn1*: in contrast to TLDA results, PCIS (and not PCLS) expressed high baseline levels of *Fn1*, and there was a significant upregulation at 48 h in PCLS.

To further explore the expression profiles of tissue slices from jejunum, liver and kidney, we measured the expression of fibrosis markers by Western blot (Fig. 4b). We observed an increased protein expression of α-SMA and HSP47 after 48 h in all tissue slices, although the increase of HSP47 in PCLS did not reach statistical significance (fold change 2.77 ± 1.90). In PCIS, even though *Acta2* mRNA expression

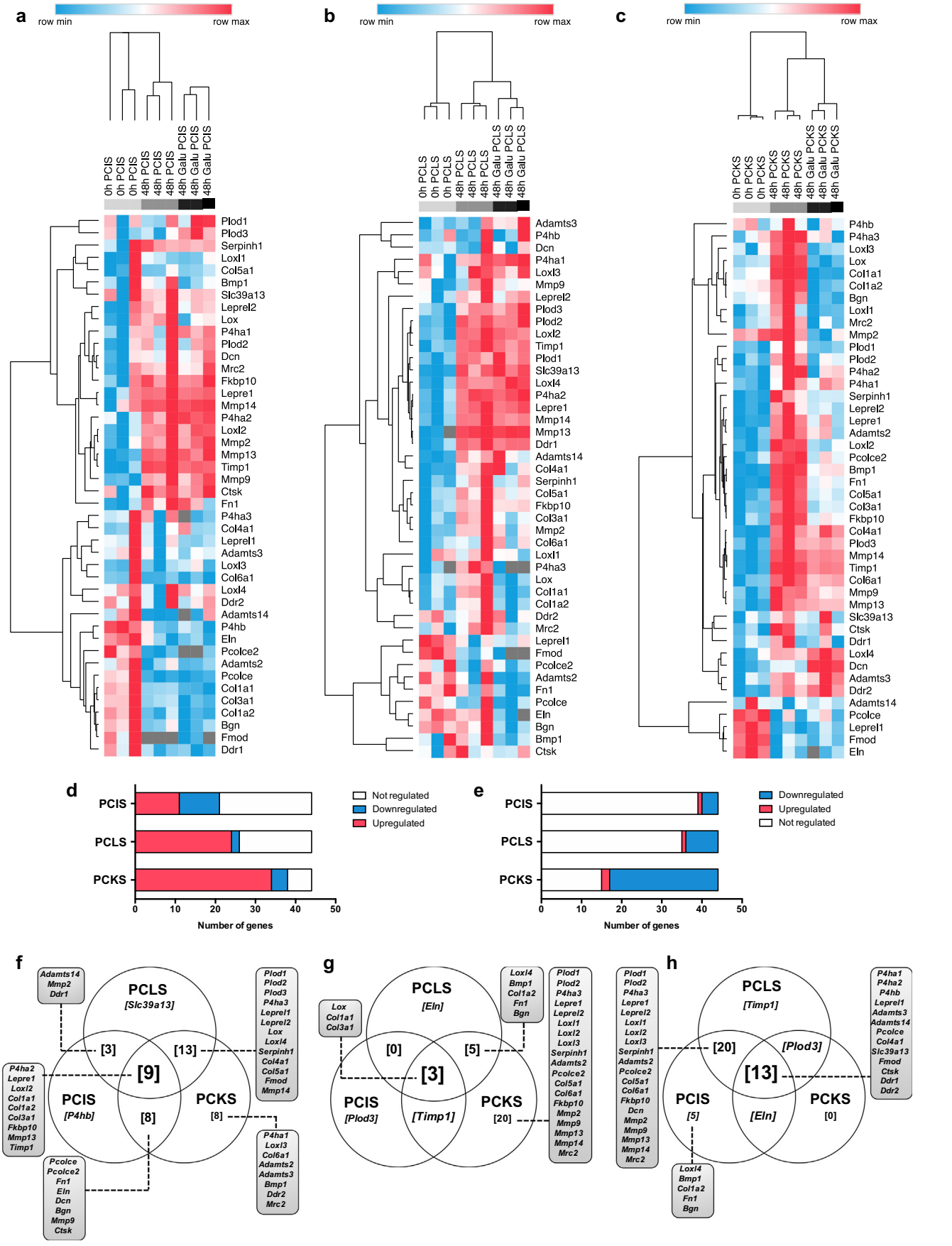

(caption on next page)

Fig. 3. Transcriptional analysis of murine precision-cut tissue slices after 48 h culture or treatment with galunisertib. (a–c) Heatmaps of the results of TaqMan low-density array (TLDA) analysis illustrating $\log_2$ fold changes in the expression of extracellular matrix related genes in PCIS (a), PCLS (b) and PCKS (c) after 48 h culture or treatment with 10 μM galunisertib. Fold changes displayed in these heatmaps were calculated as relative to the average expression in the corresponding 0 h control slices. Red and blue indicate relatively high and low expression, respectively (grey color indicates undetermined values). Row min and max expression levels were determined for each row separately, therefore min and max values are unique for each analyzed gene. Unsupervised clustering analysis is performed by average-linkage clustering method using Pearson correlation; n = 3. Fold changes and results of the statistical analyses are shown in Supplementary Table S5. (d–e) Number of genes that were not regulated or statistically significantly altered in expression in PCIS, PCLS and PCKS during 48 h culture (d) and due to the treatment with 10 μM galunisertib (e). (f–h) Venn diagrams illustrating the overlapping and unique genes among PCTS that were differentially regulated during 48 h culture (f), were affected by 10 μM galunisertib (g) or remained unchanged after the treatment (h).

was reduced at 48 h, the protein expression of α-SMA showed a significant increase. These results indicate that the fibrogenesis was not only active on a transcriptional, but also on a translational level.

Galunisertib (10 μM) mitigated the culture-induced onset of fibrogenesis in PCKS, as reflected by the dramatically reduced mRNA levels of all tested markers (Fig. 4a). Treatment affected the expression of three markers in PCLS, namely *Col1a1*, *Acta2* and *Fn1*, and it only inhibited *Col1a1* expression in PCIS. These qPCR results were in line with the TLDA. On a protein level, galunisertib showed less pronounced effects: it only significantly decreased α-SMA expression in PCLS and HSP47 expression in PCKS (Fig. 4b).

To strengthen the evidence that fibrogenic response in tissue slices is influenced by the organ type, we evaluated mRNA expression of *Col1a1*, *Acta2*, *Serpinh1* and *Fn1* in slices prepared from fibrotic livers (Supplementary Fig. S1). For this purpose, two mouse models of liver fibrosis were used to generate fibrotic PCLS, namely Mdr2 (Abcb4)−/− FVB mice that develop spontaneous biliary fibrosis [35] and Balb/c mice with induced parenchymal liver fibrosis by the administration of CCl_4 [36]. We showed that diseased PCLS displayed a clear fibrotic genotype prior to culturing: PCLS prepared from fibrotic livers had significantly higher baseline expression of all four markers (except for *Acta2* in PCLS-CCl_4) compared to PCLS prepared from livers of control mice (Supplementary Fig. S1a and c). Furthermore, fibrotic PCLS from Mdr2−/− and CCl_4-treated mice showed similarities in responses to culture and exposure to galunisertib not only between these two models of liver fibrosis but also compared to the responses in PCLS obtained from healthy mice. For instance, similar to healthy PCLS, 48 h culture induced upregulation of *Col1a1*, *Serpinh1* and *Fn1*, and galunisertib inhibited expression of *Col1a1* and *Acta2*, in all fibrotic slices (Supplementary Fig. S1b and d). Some differences were observed as well: in contrast to healthy PCLS, fibrotic slices obtained from CCl_4-treated mice showed increased levels of *Acta2* during culture, while PCLS from Mdr2−/− mice showed no response in *Fn1* mRNA expression to the treatment with galunisertib. These deviations might stem from the differences in the mouse strains, etiology of liver fibrosis and from the pre-existing diseased state of fibrotic PCLS. Nevertheless, the partial overlap in the expression of these four markers between healthy and fibrotic PCLS indicates that organ type largely dictates the responses of tissue slices to pro-fibrotic stimuli as well as to the antifibrotic treatment.

Since inflammation often accompanies fibrogenesis, we measured the gene expression of several inflammation markers, such as *Il-1b*, *Il-6*, *Cxcl1* and *Tnf* (Supplementary Fig. S2). Tissue slices exhibited differential basal expression of these profibrotic cytokines. For instance, PCIS at 0 h highly expressed *Il-6* and *Tnf*, while PCLS had significantly higher levels of *Cxcl1*. Culturing for 48 h induced a strong inflammatory response in all organs, while the treatment with galunisertib had no or little effect on the expression of the tested inflammation markers.

3.3. Involvement of canonical and non-canonical TGFβ pathway in fibrogenesis in PCTS

As mentioned above, TGFβ signalling is an essential element of organ fibrosis. Therefore, we investigated the involvement of the TGFβ pathway in the culture-induced onset of fibrogenesis in PCTS by measuring mRNA expression of *Tgfb1*, *Tgfbr1* and *Serpine1* (Fig. 5a). The latter encodes for plasminogen activator inhibitor 1 (PAI-1), which is tightly regulated by TGFβ and in fibrotic tissues promotes excessive collagen deposition [37]. Regarding baseline expression of TGFβ pathway markers, PCIS showed high levels of *Tgfb1*, PCKS had distinctly high levels of *Serpine1*, and there was no difference in expression of *Tgfbr1* between the organs. As expected, all three markers were significantly upregulated during 48 h culture in PCLS and PCKS, confirming the active involvement of the TGFβ pathway in the onset of fibrosis. PCIS also showed an increase in mRNA levels of *Tgfb1* and *Serpine1* (at a lower degree as compared to PCKS), but the *Tgfbr1* expression remained unchanged. Treatment with the TGFβR1 kinase inhibitor galunisertib only effectively blocked the TGFβ pathway in PCKS, while it failed to affect the gene expression of all three markers in PCLS and PCIS.

Since the activated TGFβRII-TGFβI/ALK5 complex phosphorylates SMAD2 (pSMAD2) [16], the changes in pSMAD2 can be used to determine the activity of the TGFβ pathway as well as the efficacy of TGFβ inhibitors. Along with pSMAD2, we measured the protein expression of pSMAD1 – the downstream molecule of TGFβRI/ALK1 signalling [38]. As predicted, pSMAD2 was significantly increased during culture to a similar degree in all organs (Fig. 5b). Interestingly, pSMAD1 was also increased in PCKS and PCIS, but not in PCLS. We noticed that in PCIS, 48 h culture induced a much more pronounced change in pSMAD1 protein expression (fold change 92.75 ± 57.72) than in pSMAD2 (fold change 6.72 ± 1.31). Treatment with 10 μM galunisertib inhibited the phosphorylation of SMAD2 in all tissue slices, without affecting pSMAD1.

To explore the activity of non-canonical TGFβ pathways in PCTS, we measured mRNA expression of *Traf6*, *Map3k7*, *Mapk1*, *Rock1* and *Rock2* (Fig. 6). TGFβ promotes K63 polyubiquitination of tumor necrosis factor receptor-associated factor 6 (TRAF6) that activates TGFβ-associated kinase 1 (TAK1) encoded by *Map3k7*, which are specifically required for activating JNK, p38 and NF-kB [18,39]. In turn, *Mapk1* encodes ERK2 – a kinase involved in TGFβ-induced ERK-MAPK signalling. Rho-associated kinases ROCK1 and ROCK2 are the downstream targets of the small GTPases RhoA, RhoB, and RhoC. The baseline mRNA expression of tested markers was significantly higher in PCIS compared to other tissue slices, except for *Traf6*, of which baseline expression was similar in all organs. Furthermore, culture-induced TGFβ activated MAPK, NF-kB and Rho-like GTPases signalling cascades in PCLS and PCKS, as reflected by significant increase in gene expression of all five markers. The effect in PCIS was the opposite: *Mapk1* and *Rock1* were downregulated at 48 h, other transcripts also showed a decreased expression, although not statistically significant. As expected, galunisertib had no impact on activation of non-canonical pathways.

3.4. Transcription factors in PCTS

Lastly, we attempted to identify which transcription factors (TFs) are involved in the onset of fibrosis in PCTS. TFs are a large family of proteins that control the transcription of genes, and are often expressed in a tissue and stress-specific manner. We measured mRNA expression of four TFs, namely *Yy1*, *Nfkb1*, *Stat3*, and *Egr1* (Fig. 7). These TFs are of interest due to their established connection to ECM regulation or TGFβ signalling. Briefly, Ying Yang 1 (YY1) protein is involved in the transcription of α1 and α2 collagen type I gene [40,41]. Early growth

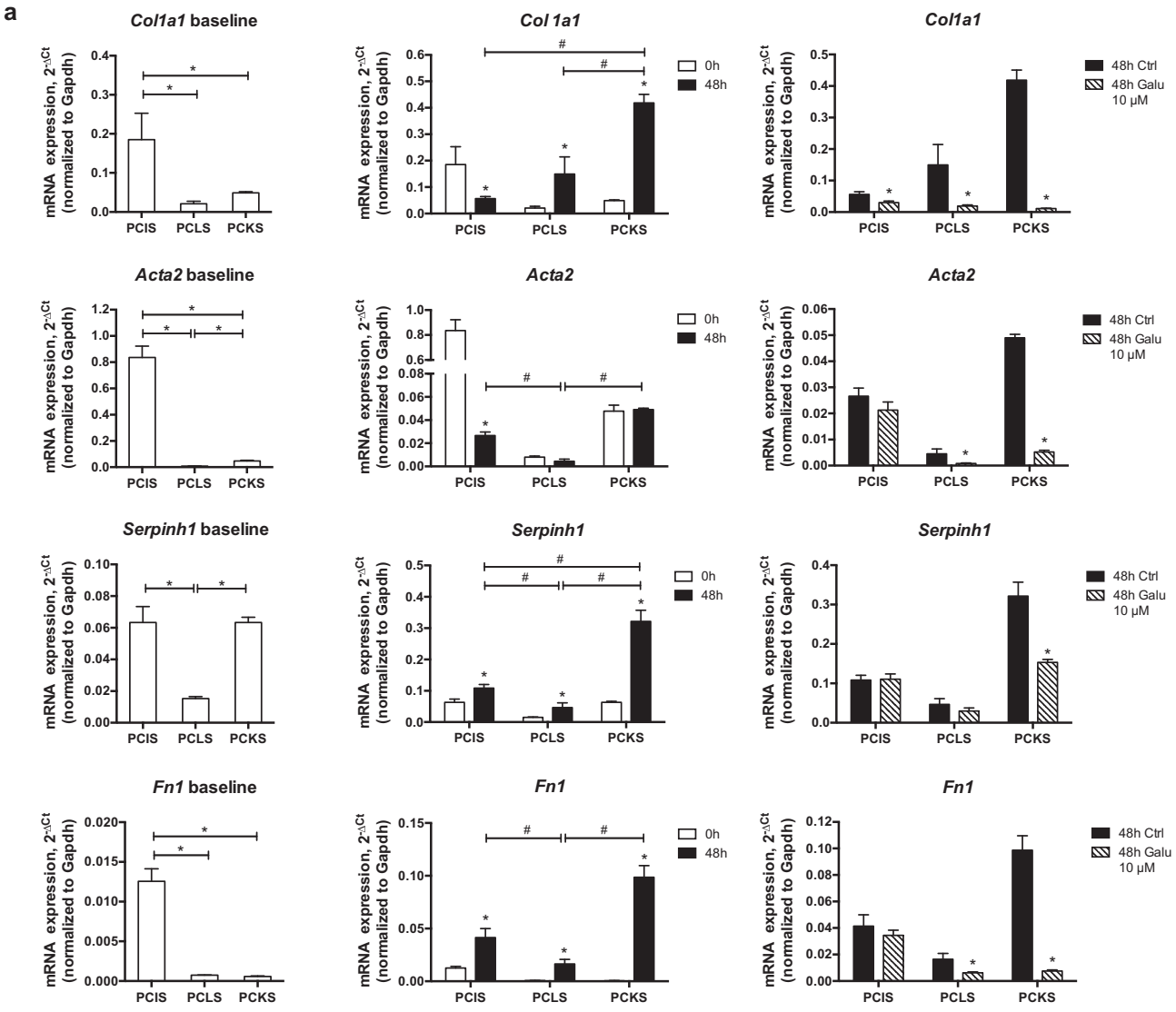

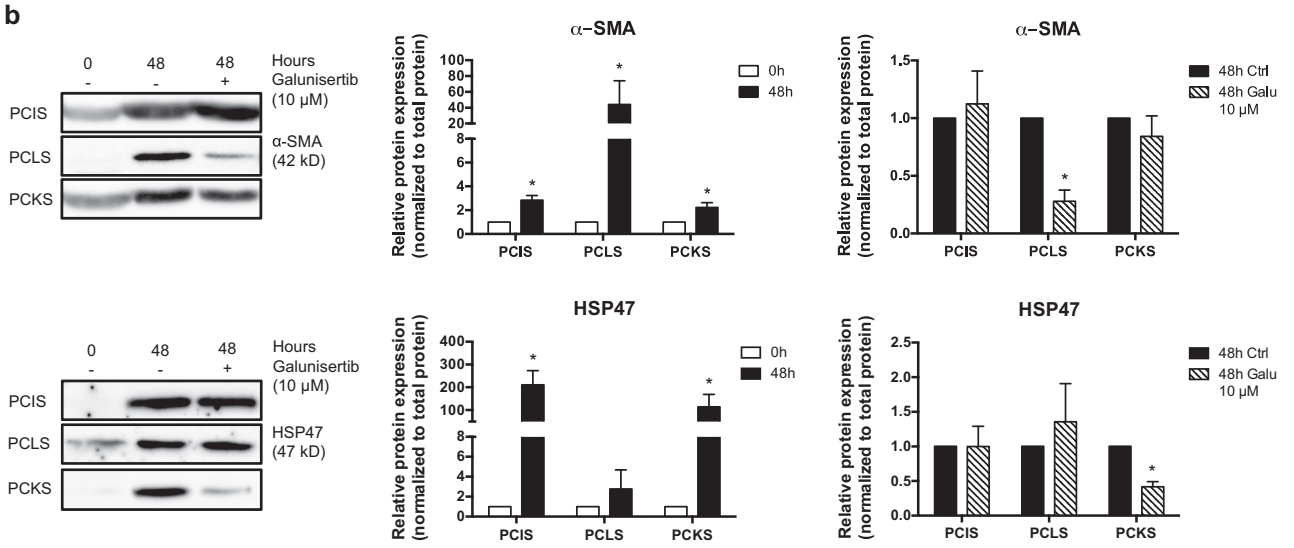

(caption on next page)

Fig. 4. Baseline expression, culture-induced effects and impact of TGFβRI/ALK5 inhibitor on markers of fibrogenesis in murine precision-cut tissue slices. (a) Expression of *Col1a1*, *Acta2*, *Serpinh1* and *Fn1* mRNA levels were measured by RT-qPCR in PCIS, PCLS and PCKS at 0 h (baseline), after 48 h culture or treatment with 10 μM galunisertib. Results are shown as $2^{-\Delta Ct}$ values normalized to *Gapdh*. Data are presented as mean ± SEM, n = 3. (*) denotes statistical differences in baseline levels or differences between 0 h and 48 h slices of the same organ, while ($^{\#}$) denotes statistical differences between slices from different organs at 48 h; $p < 0.05$. (b) Protein expression levels of α-SMA and HSP47 were examined in by Western blot. Representative gel electrophoresis bands are shown along with the quantification results of densitometry. Protein expression was normalized for total protein load and expressed as relative value to the control group. Data are presented as mean ± SEM, n = 4–5, *$p < 0.05$.

response-1 (EGR-1) also mediates TGFβ-induced collagen type I transcription, although in a SMAD-independent manner involving MAPK-ERK signalling [42,43]. In turn, TGFβ-mediated activity of NF-kB often requires cooperation with SMADs as transcriptional coactivators to regulate the transcription of its target genes [44], whereas activation of the signal transducer and activator of transcription 3 (STAT3) by TGFβ requires integrated signals from phosphorylated SMAD3 and non-canonical kinases such as JAK1 [45].

Culturing for 48 h resulted in marked upregulation of all tested TFs in PCLS and PCKS. In contrast, PCIS only displayed a culture-induced upregulation of *Egr1*, while expression of other TFs remained unchanged. The 48 h treatment with galunisertib attenuated culture-induced activation of transcription factors *Nfkb1*, *Stat3* and *Yy1* in PCLS and PCKS, but not in PCIS. Gene expression of *Egr1* remained unchanged in tissue slices after 48 h treatment.

4. Discussion

In this article, we investigated the heterogeneity of organ fibrosis. To this end, we prepared murine precision-cut tissue slices from intestine, liver and kidneys and studied changes in ECM homeostasis, onset of inflammation and fibrosis and activation of TGFβ signalling prior to culturing, after 48 h of culture or following the treatment with galunisertib, a TGFβRI/ALK5 kinase inhibitor. We provide evidence that, despite the many common features of fibrotic diseases, each organ responds differently to injury and, thus may not have similar susceptibility to antifibrotic therapy.

At baseline, precision-cut tissue slices displayed substantial organ differences, as a total of 70% of ECM-related transcripts were found to be differentially expressed in mouse intestine, liver and kidney. These differences may arise from fibroblast phenotypic heterogeneity [46,47] or from the fact that cell type composition varies between these organs, as well as the sources of myofibroblasts [48]. The baseline profile may impact further responses of the slices during culture.

Slice preparation, which entails cold ischemia and mechanic trauma, and culturing have a great impact on tissue slices: mouse intestinal, liver and kidney slices show extensive changes in ECM regulation and develop early fibrogenic as well as inflammatory responses after 48 h incubation. Similar culture-induced responses were previously reported in PCIS [20], PCLS [49] and PCKS [24]. In this study, we demonstrate that the magnitude of these changes varies by tissue type: culture-induced effects were most pronounced in PCKS and the least in PCIS. Matrix remodelling is a critical component of fibrosis [4], and our results show that all tested organ slices shared culture-induced changes in the gene expression of collagen type I (α1 and α2) and III, fibronectin, LOXL2, an enzyme that promotes collagen production [50], as well as HSP47 and FKBP65 that act as chaperones of type I collagen [51,52], among others. All tissue slices also showed a dramatic upregulation of *Mmp13* and *Timp1*, further suggesting extensive matrix remodelling during culture, as it has been shown that TIMP1 is upregulated during fibrogenesis in mouse models and in humans [53–55] and increased levels of MMP13 promote fibrosis [56–58]. Exposure of PCTS to 80% oxygen during culture also leads to an increased production of reactive oxygen species (ROS). In this case, it is likely that the oxidative stress also contributes to the onset of spontaneous inflammation and fibrogenesis in PCTS; however, the exact role of ROS and oxidative stress in the PCTS model requires further investigation.

Despite the shared similarities in ECM regulation, culture-induced changes in intestinal slices markedly differed from the other tissue slices. The majority of the studied genes were upregulated in PCLS and PCKS, whereas nearly half of the transcripts were alternatively regulated in PCIS. For instance, genes encoding collagen type I (α1 and α2), type III and alpha-SMA were among those with reduced expression in PCIS during culture. Collagen is secreted as a soluble procollagen molecule with an NH_2- (N) and a COOH (C)-terminal propeptide, and the removal of these propeptides is essential for the formation of insoluble collagen fibers [59]. Bone morphogenic protein (BMP) 1 enzymatically cleaves the C-terminal propeptide [60], while two enhancer proteins – procollagen C-endopeptidase enhancer (PCOLCE) 1 and 2 – increase catalytic activity of BMP-1 for fibrillar procollagens *in vitro* [61,62]. BMP-1 expression increases in response to fibrotic deposition of collagen [63]; however our study showed that intestinal expression of *Bmp1* remained unchanged during culture. Furthermore, expression of both *Pcolce* and *Pcolce2* were downregulated in PCIS at 48 h. These observations contradict the published work that reported on increased mRNA levels of collagen type I, III and V in fibroblasts isolated from patients with Crohn's disease [64,65]. Regarding the expression of α-SMA in PCIS, the discordance between its gene and protein levels at 48 h could be attributed to the differences in rate of transcriptional and translational processes and/or the half-lives of transcripts and proteins [66]. Further elucidation of the mechanisms of collagen type I and α-SMA transcriptional regulation in PCIS is, therefore, needed.

As a part of our interest in elucidating inter-organ differences, we investigated one of the core fibrosis pathways – the TGFβ pathway. TGFβ pathway was activated during culture in all tissue slices; however, the involvement of canonical (SMAD-dependent) and non-canonical (SMAD-independent) signalling cascades was different across the organs. In PCLS and PCKS, all tested TGFβ-mediated pathways were activated during culture, namely TGFβRI/ALK5/SMAD2, MAPK-JNK/p38/ERK, NF-kB and Rho-like GTPases. In contrast, in PCIS, only the canonical TGFβ signalling cascade was actively involved in the onset of fibrosis. Furthermore, among all tissue slices, PCIS displayed a stronger culture-induced activation of TGFβRI/ALK1/SMAD1 than of ALK5/SMAD2. There is an increasing number of studies reporting that the TGFβRI/ALK1/SMAD1 pathway is involved in organ fibrosis [38]. TGFβ signalling *via* ALK1 receptor and SMAD1, SMAD5 and SMAD8 promotes endothelial proliferation and migration and acts as an antagonistic mediator of ALK5/SMAD2/3-induced ECM protein expression [67,68]. It has been reported that ALK1 inhibits, while ALK5 potentiates, TGFβ-induced SMAD2-dependent transcriptional activity and the expression of ECM components in human chondrocytes and endothelial cells [69,70]. Therefore, it might be possible that high activity of TGFβRI/ALK1/SMAD1 signalling in PCIS plays a role in the observed downregulation of ECM- and fibrosis-related genes in PCIS during culture.

The treatment with galunisertib selectively blocked SMAD2 phosphorylation in all tissue slices, regardless of the organ of origin, without affecting pSMAD1 or non-canonical TGFβ signalling cascades. However, galunisertib only reduced the expression of the TGFβ pathway markers (*Tgfb1*, *Tgfbr1* and *Serpine1*) in PCKS, but not in PCLS or PCIS. Recently, Luangmonkong et al. reported that 10 μM galunisertib blocked SMAD2 phosphorylation in rat and human PCLS, but affected *Tgfb1* expression only in human liver slices [22]. Of note, this study also investigated the effects of TGFβ1 on rat and human PCLS

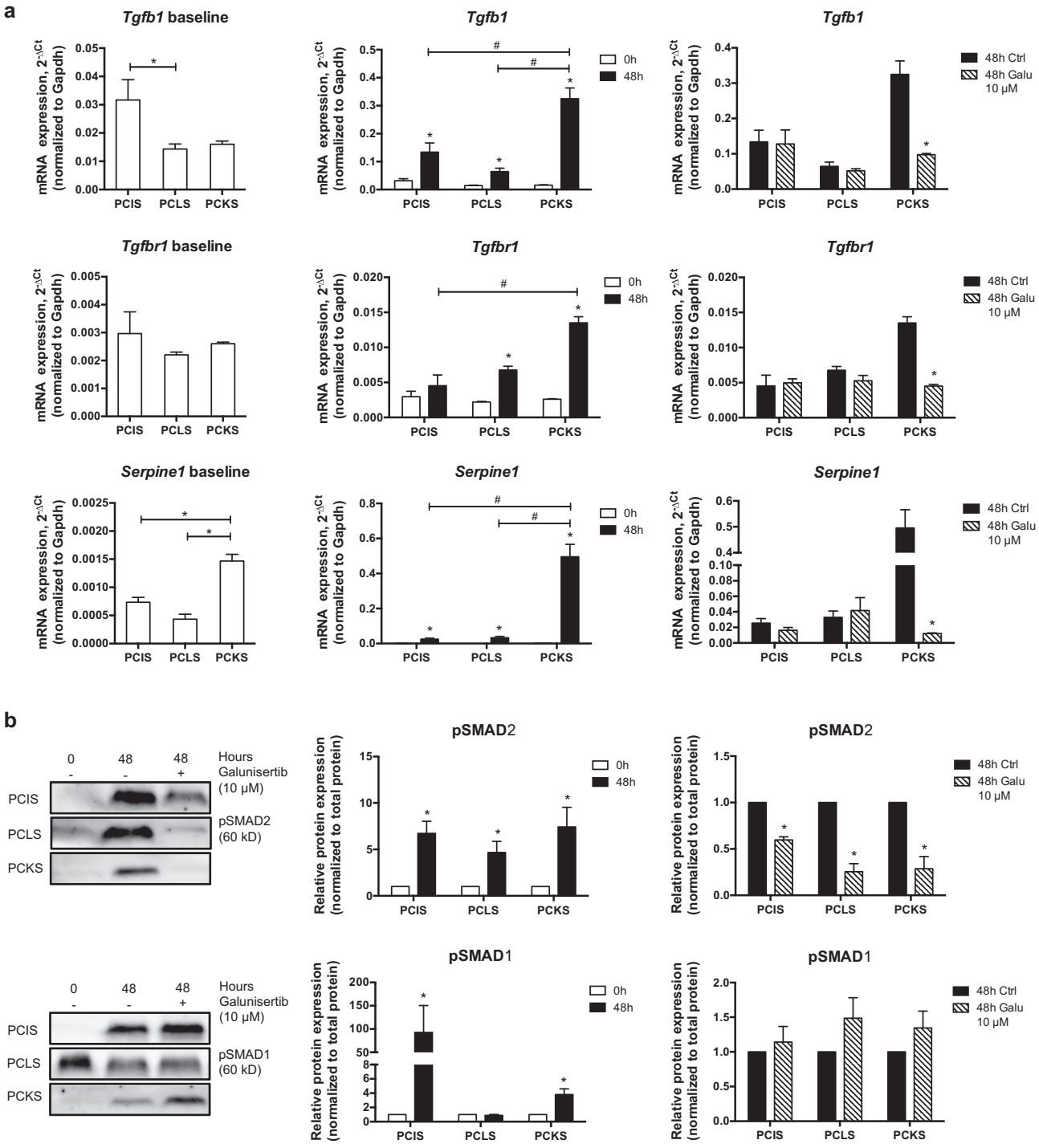

Fig. 5. Baseline expression, culture-induced effects and impact of TGFβRI/ALK5 inhibitor on TGFβ signalling in murine precision-cut tissue slices. (a) Expression of *Tgfb1*, *Tgfbr1* and *Serpine1* mRNA levels were measured by RT-qPCR in PCIS, PCLS and PCKS at 0 h (baseline), after 48 h culture or treatment with 10 μM galunisertib. Results are shown as $2^{-\Delta Ct}$ values normalized to *Gapdh*. Data are presented as mean ± SEM, n = 3. (*) denotes statistical differences in baseline levels or differences between 0 h and 48 h slices of the same organ, while (#) denotes statistical differences between slices from different organs at 48 h; $p < 0.05$. (b) Protein expression levels of pSMAD2 and pSMAD1 were examined in by Western blot. Representative gel electrophoresis bands are shown along with the quantification results of densitometry. Protein expression was normalized for total protein load and expressed as relative value to the control group. Data are presented as mean ± SEM, n = 4–5, *$p < 0.05$.

during culture and in presence of galunisertib. Studies on hepatocellular carcinoma also found a significant reduction of *Tgfb1* and *Tgfbr1* mRNA levels by galunisertib *in vivo* in mice and *ex vivo* in human tumor tissue [71,72]. These findings suggest that along with organ-differences, the effect of galunisertib varies between species and is possibly more pronounced in tissues with an established pathological state.

Following the observation that galunisertib downregulated *Tgfb1*, *Tgfbr1* and *Serpine1* only in kidney slices, our results demonstrate that galunisertib mitigated culture-induced changes in ECM homeostasis and early fibrogenesis most effectively in PCKS, showed moderate activity in PCLS and had only limited effect in PCIS. Most of the tested ECM- and fibrosis-related genes seem to operate in a TGFβRI/ALK5/

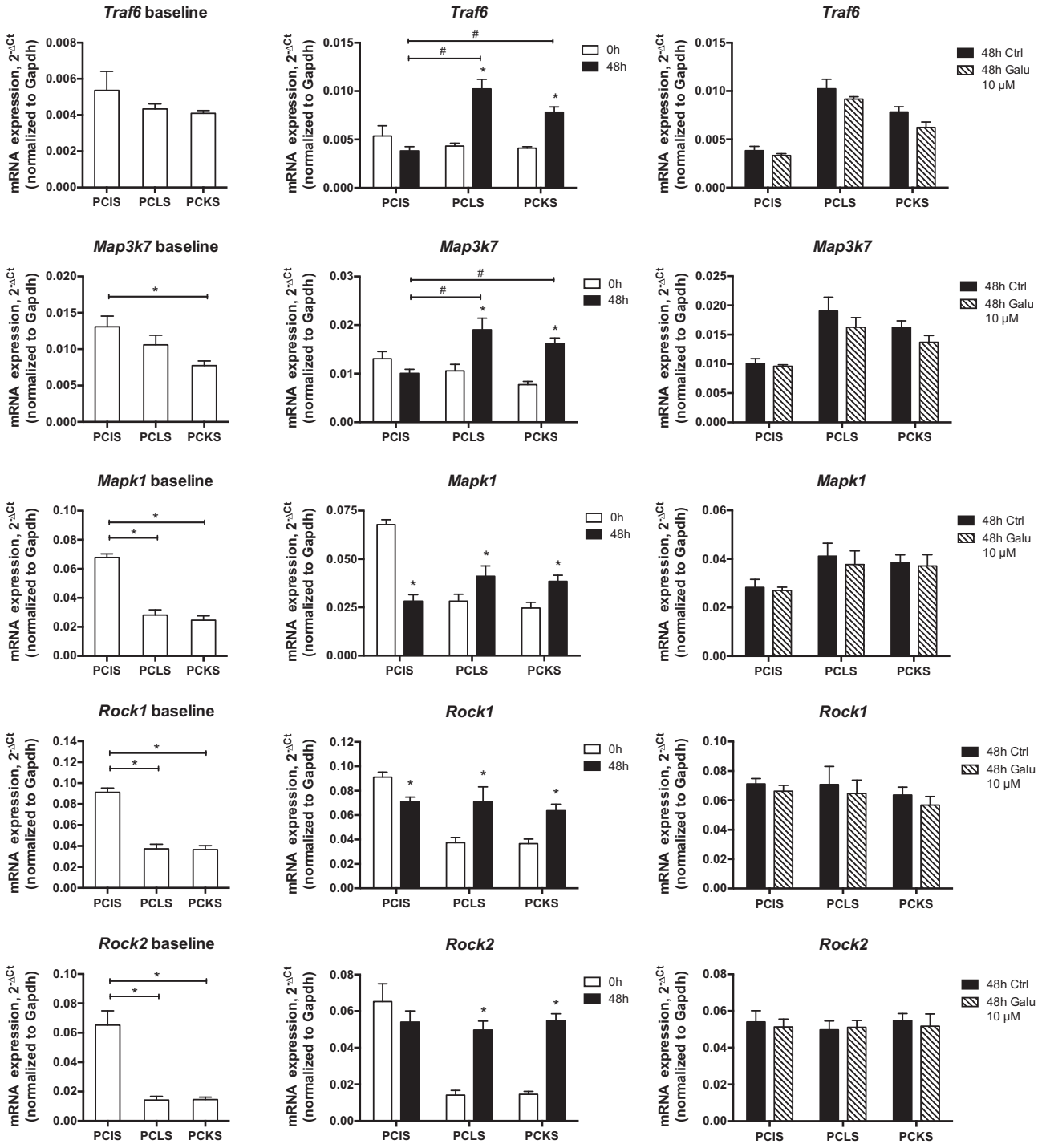

Fig. 6. Baseline expression, culture-induced effects and impact of TGFβRI/ALK5 inhibitor on non-canonical TGFβ signalling in murine precision-cut tissue slices. Expression of *Traf6*, *Map3k7*, *Mapk1*, *Rock1* and *Rock2* mRNA levels were measured by RT-qPCR in PCIS, PCLS and PCKS at 0 h (baseline), after 48 h culture or treatment with 10 μM galunisertib. Results are shown as $2^{-\Delta Ct}$ values normalized to *Gapdh*. Data are presented as mean ± SEM, n = 3. (*) denotes statistical differences in baseline levels or differences between 0 h and 48 h slices of the same organ, while ($^{\#}$) denotes statistical differences between slices from different organs at 48 h; $p < 0.05$.

SMAD2 dependent manner in kidney, but not in intestine, emphasizing that ECM homeostasis and early fibrogenesis are regulated differently in these organs. Notably, *ex vivo* activity of galunisertib in PCLS (healthy and fibrotic) falls in line with recent *in vivo* studies that showed antifibrotic potency of galunisertib in liver fibrosis, which was mainly associated with ECM remodelling [73,74]. We speculate that similarly, antifibrotic effects of galunisertib in PCKS might translate into mitigation of renal fibrosis *in vivo*.

Interestingly, while galunisertib inhibited mRNA expression of collagen type I (α1) and III in all tissue slices, the treatment had no impact on collagen type IV as well as on *Leprel1* gene, encoding P3H enzyme responsible for modifying type IV collagens [75]. Different types of collagen vary in their structure, assembly and function. Types I and III collagens belong to the family of fibril-forming collagens that are largely present in ECM, whereas type IV collagen is the main structural component of basement membranes [76]. The regulation of these

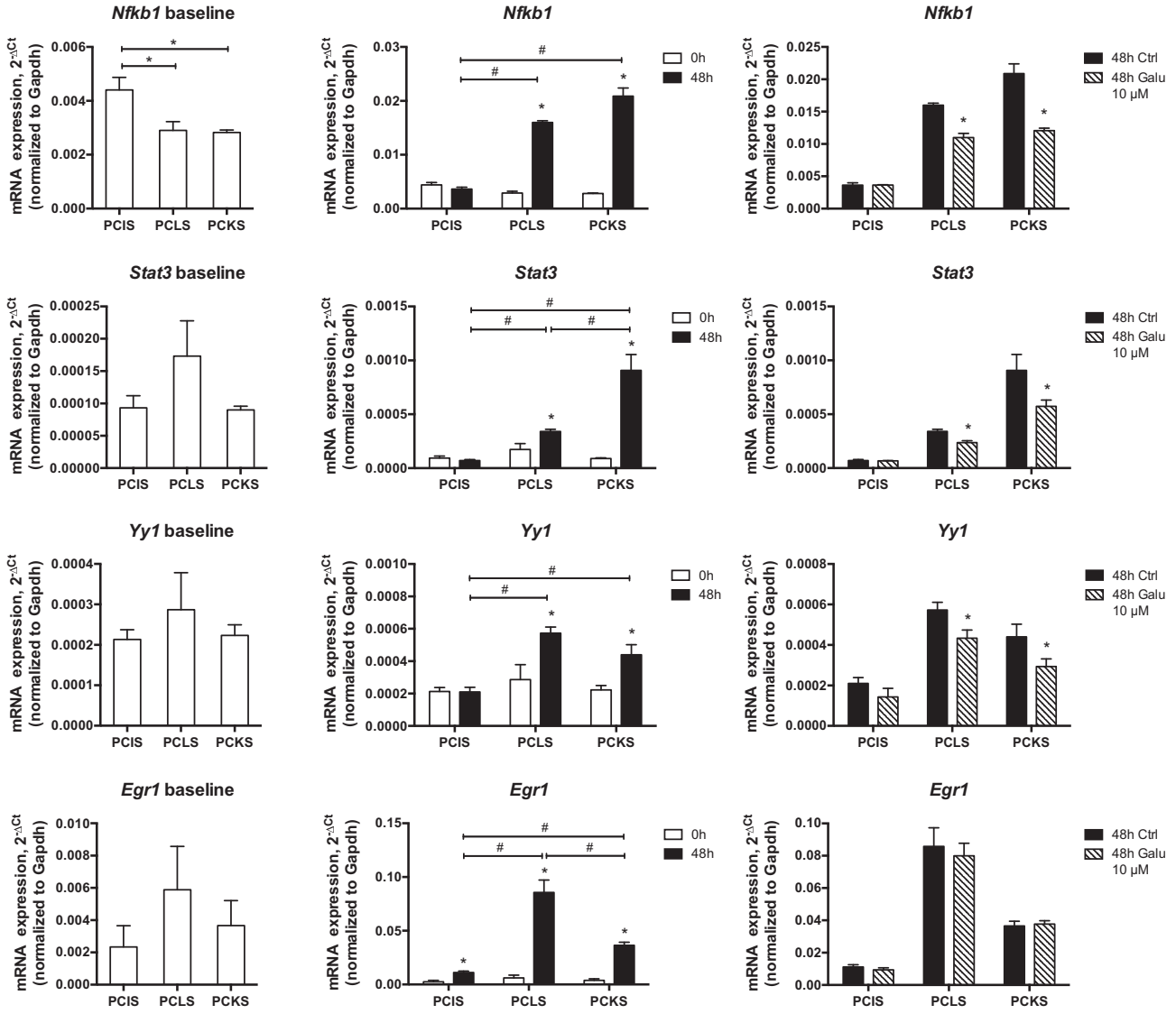

Fig. 7. Regulation of selected transcription factors in murine precision-cut tissue slices. Expression of *Nfkb1*, *Stat3*, *Yy1* and *Egr1* mRNA levels were measured by RT-qPCR in PCIS, PCLS and PCKS at 0 h (baseline), after 48 h culture or treatment with 10 μM galunisertib. Results are shown as $2^{-\Delta Ct}$ values normalized to *Gapdh*. Data are presented as mean ± SEM, n = 3. (*) denotes statistical differences in baseline levels or differences between 0 h and 48 h slices of the same organ, while (#) denotes statistical differences between slices from different organs at 48 h; $p < 0.05$.

collagen types also differs in tissue slices, as expression of *Col4a1* seems to be TGFβ-independent, in contrast to *Col1a1* and *Col3a1*.

In addition, we investigated the expression of several transcriptional factors (TFs) in PCTS during culture and after galunisertib treatment. Guo et al. demonstrated that TGFβ induced the expression of YY1 in lung fibroblasts, which in turn can directly regulate αSMA and collagen expression [77]. We did not observe an increase in *Yy1* expression in PCIS during culture; this could explain the absence of induction of the expression of *Col1a1* and *Acta2* during culture. In general, TFs that operate in a SMAD-dependent manner (*Yy1*, *Stat3*, *Nfkb1*) were affected by galunisertib treatment in both PCLS and PCKS, while those that are SMAD-independent (*Egr1*) were not.

5. Conclusion

Taken together, our study details the organ-specific features of fibrosis in murine intestine, liver and kidney slices. PCTS, as an *ex vivo* fibrosis model, reflects the diversity of the responses that are specific to the organ and species. Furthermore, our results revealed that treatment with TGFβRI/ALK5 kinase inhibitor elicits varying effects in PCTS, confirming that organs do not display similar susceptibility to anti-fibrotic therapy, even though it targets a core fibrosis pathway. The following limitations of the PCTS model have to be considered: (1) relatively short culture period might not fully demonstrate changes on a translational level; (2) influence of the immune system cannot be directly assessed and (3) complexity of a multi-organ system cannot be replicated. Our findings provide the foundation for future investigations of the unique organ features within the common pathology – fibrosis. A better understanding of the processes and mechanisms that contribute to organ fibrosis may stimulate a hybrid approach for the drug development – targeting core fibrosis-regulating factors in an organ-specific manner. Therefore, new in-depth studies of precision-cut tissue slices of mouse and human origin using advanced genomic and proteomic technologies, among others, are needed.

Transparency document

The Transparency document associated this article can be found, in online version.

Declaration of competing interest

The authors declare that they have no known competing financial interests or personal relationships that could have appeared to influence the work reported in this paper.

Acknowledgements

The present study was kindly supported by ZonMw (the Netherlands Organization for Health Research and Development), grant number 114025003.

Author contributions

E.B., M.B. and P.O. designed the study; E.B., and E.G. carried out experiments with the help of D.O. and analyzed the data; D.S. and Y.O.K. provided access and assisted with mouse models of liver fibrosis; R.A.B provided custom designed TLDA; E.B. wrote the manuscript with critical review from H.A.M.M., D.S., R.A.B., M.B. and P.O. All of the authors approved the final version of the manuscript for publication.

Appendix A. Supplementary data

Supplementary data to this article can be found online at https://doi.org/10.1016/j.bbadis.2019.165582.

References

[1] D.C. Rockey, P.D. Bell, J.A. Hill, Fibrosis — a common pathway to organ injury and failure, N. Engl. J. Med. 372 (2015) 1138–1149, https://doi.org/10.1056/NEJMra1300575.
[2] T.A. Wynn, T.R. Ramalingam, Mechanisms of fibrosis: therapeutic translation for fibrotic disease, Nat. Med. 18 (2012) 1028–1040, https://doi.org/10.1038/nm.2807.
[3] L. Schaefer, Decoding fibrosis: mechanisms and translational aspects, Matrix Biol. 68–69 (2018) 1–7, https://doi.org/10.1016/j.matbio.2018.04.009.
[4] C.B. Nanthakumar, R.J.D. Hatley, S. Lemma, J. Gauldie, R.P. Marshall, S.J.F. Macdonald, Dissecting fibrosis: therapeutic insights from the small-molecule toolbox, Nat. Rev. Drug Discov. 14 (2015) 693–720, https://doi.org/10.1038/nrd4592.
[5] K.E. Wenzke, C. Cantemir-Stone, J. Zhang, C.B. Marsh, K. Huang, Identifying common genes and networks in multi-organ fibrosis, AMIA Jt. Summits Transl. Sci. Proceedings. AMIA Jt. Summits Transl. Sci. 2012 (2012) 106–115 http://www.ncbi.nlm.nih.gov/pubmed/22779061.
[6] T. Wynn, Cellular and molecular mechanisms of fibrosis, J. Pathol. 214 (2008) 199–210, https://doi.org/10.1002/path.2277.
[7] A. Pardo, Matrix metalloproteases in aberrant fibrotic tissue remodeling, Proc. Am. Thorac. Soc. 3 (2006) 383–388, https://doi.org/10.1513/pats.200601-012TK.
[8] M. Zeisberg, R. Kalluri, Cellular mechanisms of tissue fibrosis. 1. Common and organ-specific mechanisms associated with tissue fibrosis, Am. J. Physiol. Physiol. 304 (2013) C216–C225, https://doi.org/10.1152/ajpcell.00328.2012.
[9] M. Mack, Inflammation and fibrosis, Matrix Biol. 68–69 (2018) 106–121, https://doi.org/10.1016/j.matbio.2017.11.010.
[10] R. Weiskirchen, S. Weiskirchen, F. Tacke, Organ and tissue fibrosis: molecular signals, cellular mechanisms and translational implications, Mol. Asp. Med. 65 (2019) 2–15, https://doi.org/10.1016/j.mam.2018.06.003.
[11] D. Pohlers, J. Brenmoehl, I. Löffler, C.K. Müller, C. Leipner, S. Schultze-Mosgau, A. Stallmach, R.W. Kinne, G. Wolf, TGF-β and fibrosis in different organs — molecular pathway imprints, Biochim. Biophys. Acta - Mol. Basis Dis. 1792 (2009) 746–756, https://doi.org/10.1016/j.bbadis.2009.06.004.
[12] A.H. Györfi, A.-E. Matei, J.H.W. Distler, Targeting TGF-β signaling for the treatment of fibrosis, Matrix Biol. 68–69 (2018) 8–27, https://doi.org/10.1016/j.matbio.2017.12.016.
[13] T. Kisseleva, D.A. Brenner, Fibrogenesis of parenchymal organs, Proc. Am. Thorac. Soc. 5 (2008) 338–342, https://doi.org/10.1513/pats.200711-168DR.
[14] A. Mauviel, Transforming growth factor-β: a key mediator of fibrosis, Methods Mol. Med. 117 (2005) 69–80, https://doi.org/10.1385/1-59259-940-0:069.
[15] F. Rieder, C. Fiocchi, Intestinal fibrosis in inflammatory bowel disease — current knowledge and future perspectives, J. Crohn's Colitis 2 (2008) 279–290, https://doi.org/10.1016/j.crohns.2008.05.009.
[16] J. Massagué, TGFβ signalling in context, Nat. Rev. Mol. Cell Biol. 13 (2012) 616–630, https://doi.org/10.1038/nrm3434.
[17] Y.E. Zhang, Non-Smad pathways in TGF-β signaling, Cell Res. 19 (2009) 128–139, https://doi.org/10.1038/cr.2008.328.
[18] Y. Mu, S.K. Gudey, M. Landström, Non-Smad signaling pathways, Cell Tissue Res. 347 (2012) 11–20, https://doi.org/10.1007/s00441-011-1201-y.
[19] I.A. de Graaf, G.M. Groothuis, P. Olinga, Precision-cut tissue slices as a tool to predict metabolism of novel drugs, Expert Opin. Drug Metab. Toxicol. 3 (2007) 879–898, https://doi.org/10.1517/17425255.3.6.879.
[20] B.T. Pham, W.T. van Haaften, D. Oosterhuis, J. Nieken, I.A.M. de Graaf, P. Olinga, Precision-cut rat, mouse, and human intestinal slices as novel models for the early-onset of intestinal fibrosis, Physiol. Rep. 3 (2015) e12323, , https://doi.org/10.14814/phy2.12323.
[21] I.M. Westra, D. Oosterhuis, G.M.M. Groothuis, P. Olinga, The effect of antifibrotic drugs in rat precision-cut fibrotic liver slices, PLoS One 9 (2014) e95462, , https://doi.org/10.1371/journal.pone.0095462.
[22] T. Luangmonkong, S. Suriguga, E. Bigaeva, M. Boersema, D. Oosterhuis, K.P. de Jong, D. Schuppan, H.A.M. Mutsaers, P. Olinga, Evaluating the antifibrotic potency of galunisertib in a human ex vivo model of liver fibrosis, Br. J. Pharmacol. 174 (2017) 3107–3117, https://doi.org/10.1111/bph.13945.
[23] F. Poosti, B.T. Pham, D. Oosterhuis, K. Poelstra, H. van Goor, P. Olinga, J.-L. Hillebrands, Precision-cut kidney slices (PCKS) to study development of renal fibrosis and efficacy of drug targeting ex vivo, Dis. Model. Mech. 8 (2015) 1227–1236, https://doi.org/10.1242/dmm.020172.
[24] E.G.D. Stribos, M.A. Seelen, H. van Goor, P. Olinga, H.A.M. Mutsaers, Murine precision-cut kidney slices as an ex vivo model to evaluate the role of transforming growth factor-β1 signaling in the onset of renal fibrosis, Front. Physiol. 8 (2017) 1026, https://doi.org/10.3389/fphys.2017.01026.
[25] J. Rodon, M.A. Carducci, J.M. Sepulveda-Sánchez, A. Azaro, E. Calvo, J. Seoane, I. Braña, E. Sicart, I. Gueorguieva, A.L. Cleverly, N.S. Pillay, D. Desaiah, S.T. Estrem, L. Paz-Ares, M. Holdhoff, J. Blakeley, M.M. Lahn, J. Baselga, First-in-human dose study of the novel transforming growth factor-β receptor I kinase inhibitor LY2157299 monohydrate in patients with advanced cancer and glioma, Clin. Cancer Res. 21 (2015) 553–560, https://doi.org/10.1158/1078-0432.CCR-14-1380.
[26] S. Herbertz, J.S. Sawyer, A.J. Stauber, I. Gueorguieva, K.E. Driscoll, S.T. Estrem, A.L. Cleverly, D. Desaiah, S.C. Guba, K.A. Benhadji, C.A. Slapak, M.M. Lahn, Clinical development of galunisertib (LY2157299 monohydrate), a small molecule inhibitor of transforming growth factor-beta signaling pathway, Drug Des. Devel. Ther. 9 (2015) 4479–4499, https://doi.org/10.2147/DDDT.S86621.
[27] A. de Gramont, S. Faivre, E. Raymond, Novel TGF-β inhibitors ready for prime time in onco-immunology, Oncoimmunology 6 (2017) e1257453, , https://doi.org/10.1080/2162402X.2016.1257453.
[28] I.A.M. de Graaf, P. Olinga, M.H. de Jager, M.T. Merema, R. de Kanter, E.G. van de Kerkhof, G.M.M. Groothuis, Preparation and incubation of precision-cut liver and intestinal slices for application in drug metabolism and toxicity studies, Nat. Protoc. 5 (2010) 1540–1551, https://doi.org/10.1038/nprot.2010.111.
[29] I. Gueorguieva, A.L. Cleverly, A. Stauber, N. Sada Pillay, J.A. Rodon, C.P. Miles, J.M. Yingling, M.M. Lahn, Defining a therapeutic window for the novel TGF-β inhibitor LY2157299 monohydrate based on a pharmacokinetic/pharmacodynamic model, Br. J. Clin. Pharmacol. 77 (2014) 796–807, https://doi.org/10.1111/BCP.12256.
[30] J.M. Yingling, W.T. McMillen, L. Yan, H. Huang, J.S. Sawyer, J. Graff, D.K. Clawson, K.S. Britt, B.D. Anderson, D.W. Beight, D. Desaiah, M.M. Lahn, K.A. Benhadji, M.J. Lallena, R.B. Holmgaard, X. Xu, F. Zhang, J.R. Manro, P.W. Iversen, C.V. Iyer, R.A. Brekken, M.D. Kalos, K.E. Driscoll, Preclinical assessment of galunisertib (LY2157299 monohydrate), a first-in-class transforming growth factor-β receptor type I inhibitor, Oncotarget 9 (2018) 6659–6677, https://doi.org/10.18632/oncotarget.23795.
[31] C.L. Andersen, J.L. Jensen, T.F. Ørntoft, Normalization of real-time quantitative reverse transcription-PCR data: a model-based variance estimation approach to identify genes suited for normalization, applied to bladder and colon cancer data sets, Cancer Res. 64 (2004) 5245–5250, https://doi.org/10.1158/0008-5472.CAN-04-0496.
[32] K.J. Livak, T.D. Schmittgen, Analysis of relative gene expression data using real-time quantitative PCR and the $2-\Delta\Delta CT$ method, Methods 25 (2001) 402–408, https://doi.org/10.1006/METH.2001.1262.
[33] C.L. Ladner, J. Yang, R.J. Turner, R.A. Edwards, Visible fluorescent detection of proteins in polyacrylamide gels without staining, Anal. Biochem. 326 (2004) 13–20, https://doi.org/10.1016/J.AB.2003.10.047.
[34] E. Bigaeva, J.J.M. Bomers, C. Biel, H.A.M. Mutsaers, I.A.M. de Graaf, M. Boersema, P. Olinga, Growth factors of stem cell niche extend the life-span of precision-cut intestinal slices in culture: a proof-of-concept study, Toxicol. Vitr. 59 (2019) 312–321, https://doi.org/10.1016/j.tiv.2019.05.024.
[35] Y. Popov, E. Patsenker, P. Fickert, M. Trauner, D. Schuppan, Mdr2 (Abcb4) −/− mice spontaneously develop severe biliary fibrosis via massive dysregulation of pro- and antifibrogenic genes, J. Hepatol. 43 (2005) 1045–1054, https://doi.org/10.1016/j.jhep.2005.06.025.
[36] Y. Popov, D.Y. Sverdlov, A.K. Sharma, K.R. Bhaskar, S. Li, T.L. Freitag, J. Lee, W. Dieterich, G. Melino, D. Schuppan, Tissue transglutaminase does not affect fibrotic matrix stability or regression of liver fibrosis in mice, Gastroenterology 140 (2011) 1642–1652, https://doi.org/10.1053/j.gastro.2011.01.040.
[37] A.K. Ghosh, D.E. Vaughan, PAI-1 in tissue fibrosis, J. Cell. Physiol. 227 (2012) 493–507, https://doi.org/10.1002/jcp.22783.
[38] J.M. Muñoz-Félix, M. González-Núñez, J.M. López-Novoa, ALK1-Smad1/5 signaling pathway in fibrosis development: friend or foe? Cytokine Growth Factor Rev. 24 (2013) 523–537, https://doi.org/10.1016/j.cytogfr.2013.08.002.
[39] M. Yamashita, K. Fatyol, C. Jin, X. Wang, Z. Liu, Y.E. Zhang, TRAF6 mediates Smad-independent activation of JNK and p38 by TGF-beta, Mol. Cell 31 (2008) 918–924, https://doi.org/10.1016/j.molcel.2008.09.002.
[40] K. Miao, J.J. Potter, F.A. Anania, L. Rennie-Tankersley, E. Mezey, Identification of two repressor elements in the mouse alpha 2(I) collagen promoter, Arch. Biochem. Biophys. 361 (1999) 7–16, https://doi.org/10.1006/abbi.1998.0977.

[41] F.B. Riquet, L. Tan, B.K. Choy, M. Osaki, G. Karsenty, T.F. Osborne, P.E. Auron, M.B. Goldring, YY1 is a positive regulator of transcription of the Col1a1 gene, J. Biol. Chem. 276 (2001) 38665–38672, https://doi.org/10.1074/jbc.M009881200.

[42] S.-J. Chen, H. Ning, W. Ishida, S. Sodin-Semrl, S. Takagawa, Y. Mori, J. Varga, The early-immediate gene EGR-1 is induced by transforming growth factor-β and mediates stimulation of collagen gene expression, J. Biol. Chem. 281 (2006) 21183–21197, https://doi.org/10.1074/jbc.M603270200.

[43] S. Bhattacharyya, S.-J. Chen, M. Wu, M. Warner-Blankenship, H. Ning, G. Lakos, Y. Mori, E. Chang, C. Nihijima, K. Takehara, C. Feghali-Bostwick, J. Varga, Smad-independent transforming growth factor-beta regulation of early growth response-1 and sustained expression in fibrosis: implications for scleroderma, Am. J. Pathol. 173 (2008) 1085–1099, https://doi.org/10.2353/ajpath.2008.080382.

[44] T. López-Rovira, E. Chalaux, J.L. Rosa, R. Bartrons, F. Ventura, Interaction and functional cooperation of NF-kappa B with Smads. Transcriptional regulation of the junB promoter, J. Biol. Chem. 275 (2000) 28937–28946, https://doi.org/10.1074/jbc.M909923199.

[45] D. Chakraborty, B. Šumová, T. Mallano, C.-W. Chen, A. Distler, C. Bergmann, I. Ludolph, R.E. Horch, K. Gelse, A. Ramming, O. Distler, G. Schett, L. Šenolt, J.H.W. Distler, Activation of STAT3 integrates common profibrotic pathways to promote fibroblast activation and tissue fibrosis, Nat. Commun. 8 (2017) 1130, https://doi.org/10.1038/s41467-017-01236-6.

[46] K.M. Fries, T. Blieden, R.J. Looney, G.D. Sempowski, M.R. Silvera, R.A. Willis, R.P. Phipps, Evidence of fibroblast heterogeneity and the role of fibroblast subpopulations in fibrosis, Clin. Immunol. Immunopathol. 72 (1994) 283–292 http://www.ncbi.nlm.nih.gov/pubmed/7914840.

[47] J.L. Rinn, C. Bondre, H.B. Gladstone, P.O. Brown, H.Y. Chang, Anatomic demarcation by positional variation in fibroblast gene expression programs, PLoS Genet. 2 (2006) e119, https://doi.org/10.1371/journal.pgen.0020119.

[48] L. Micallef, N. Vedrenne, F. Billet, B. Coulomb, I.A. Darby, A. Desmoulière, The myofibroblast, multiple origins for major roles in normal and pathological tissue repair, Fibrogenesis Tissue Repair 5 (2012) S5, https://doi.org/10.1186/1755-1536-5-s1-s5.

[49] I.M. Westra, D. Oosterhuis, G.M.M. Groothuis, P. Olinga, Precision-cut liver slices as a model for the early onset of liver fibrosis to test antifibrotic drugs, Toxicol. Appl. Pharmacol. 274 (2014) 328–338, https://doi.org/10.1016/j.taap.2013.11.017.

[50] J. Yang, K. Savvatis, J.S. Kang, P. Fan, H. Zhong, K. Schwartz, V. Barry, A. Mikels-Vigdal, S. Karpinski, D. Kornyeyev, J. Adamkewicz, X. Feng, Q. Zhou, C. Shang, P. Kumar, D. Phan, M. Kasner, B. López, J. Diez, K.C. Wright, R.L. Kovacs, P.-S. Chen, T. Quertermous, V. Smith, L. Yao, C. Tschöpe, C.-P. Chang, Targeting LOXL2 for cardiac interstitial fibrosis and heart failure treatment, Nat. Commun. 7 (2016) 13710, https://doi.org/10.1038/ncomms13710.

[51] K. Nagata, HSP47 as a collagen-specific molecular chaperone: function and expression in normal mouse development, Semin. Cell Dev. Biol. 14 (2003) 275–282, https://doi.org/10.1016/j.semcdb.2003.09.020.

[52] Y. Ishikawa, J. Vranka, J. Wirz, K. Nagata, H.P. Bächinger, The rough endoplasmic reticulum-resident FK506-binding protein FKBP65 is a molecular chaperone that interacts with collagens, J. Biol. Chem. 283 (2008) 31584–31590, https://doi.org/10.1074/jbc.M802535200.

[53] V. Arpino, M. Brock, S.E. Gill, The role of TIMPs in regulation of extracellular matrix proteolysis, Matrix Biol. 44–46 (2015) 247–254, https://doi.org/10.1016/j.matbio.2015.03.005.

[54] H. Herbst, T. Wege, S. Milani, G. Pellegrini, H.D. Orzechowski, W.O. Bechstein, P. Neuhaus, A.M. Gressner, D. Schuppan, Tissue inhibitor of metalloproteinase-1 and -2 RNA expression in rat and human liver fibrosis, Am. J. Pathol. 150 (1997) 1647–1659 http://www.ncbi.nlm.nih.gov/pubmed/9137090.

[55] C.J. Parsons, B.U. Bradford, C.Q. Pan, E. Cheung, M. Schauer, A. Knorr, B. Krebs, S. Kraft, S. Zahn, B. Brocks, N. Feirt, B. Mei, M.-S. Cho, R. Ramamoorthi, G. Roldan, P. Ng, P. Lum, C. Hirth-Dietrich, A. Tomkinson, D.A. Brenner, Antifibrotic effects of a tissue inhibitor of metalloproteinase-1 antibody on established liver fibrosis in rats, Hepatology 40 (2004) 1106–1115, https://doi.org/10.1002/hep.20425.

[56] M. Roderfeld, Matrix metalloproteinase functions in hepatic injury and fibrosis, Matrix Biol. 68–69 (2018) 452–462, https://doi.org/10.1016/j.matbio.2017.11.011.

[57] M. Giannandrea, W.C. Parks, Diverse functions of matrix metalloproteinases during fibrosis, Dis. Model. Mech. 7 (2014) 193–203, https://doi.org/10.1242/dmm.012062.

[58] S. O'Sullivan, J.F. Gilmer, C. Medina, Matrix metalloproteinases in inflammatory bowel disease: an update, Mediat. Inflamm. 2015 (2015) 964131, https://doi.org/10.1155/2015/964131.

[59] W. McKleroy, T.-H. Lee, K. Atabai, Always cleave up your mess: targeting collagen degradation to treat tissue fibrosis, Am. J. Physiol. Cell. Mol. Physiol. 304 (2013) L709–L721, https://doi.org/10.1152/ajplung.00418.2012.

[60] E. Kessler, K. Takahara, L. Biniaminov, M. Brusel, D.S. Greenspan, Bone morphogenetic protein-1: the type I procollagen C-proteinase, Science. 271 (1996) 360–362, https://doi.org/10.1126/science.271.5247.360.

[61] K. Takahara, E. Kessler, L. Biniaminov, M. Brusel, R.L. Eddy, S. Jani-Sait, T.B. Shows, D.S. Greenspan, Type I procollagen COOH-terminal proteinase enhancer protein: identification, primary structure, and chromosomal localization of the cognate human gene (PCOLCE), J. Biol. Chem. 269 (1994) 26280–26285 http://www.ncbi.nlm.nih.gov/pubmed/7523404.

[62] B.M. Steiglitz, D.R. Keene, D.S. Greenspan, PCOLCE2 encodes a functional procollagen C-proteinase enhancer (PCPE2) that is a collagen-binding protein differing in distribution of expression and post-translational modification from the previously described PCPE1, J. Biol. Chem. 277 (2002) 49820–49830, https://doi.org/10.1074/jbc.M209891200.

[63] S. Vadon-Le Goff, D.J.S. Hulmes, C. Moali, BMP-1/tolloid-like proteinases synchronize matrix assembly with growth factor activation to promote morphogenesis and tissue remodeling, Matrix Biol. 44–46 (2015) 14–23, https://doi.org/10.1016/j.matbio.2015.02.006.

[64] A. Stallmach, D. Schuppan, H.H. Riese, H. Matthes, E.O. Riecken, Increased collagen type III synthesis by fibroblasts isolated from strictures of patients with Crohn's disease, Gastroenterology. 102 (1992) 1920–1929, https://doi.org/10.5555/URI:PII:001650859290314O.

[65] F. Rieder, J. Brenmoehl, S. Leeb, J. Schölmerich, G. Rogler, Wound healing and fibrosis in intestinal disease, Gut 56 (2007) 130–139, https://doi.org/10.1136/gut.2006.090456.

[66] B. Schwanhäusser, D. Busse, N. Li, G. Dittmar, J. Schuchhardt, J. Wolf, W. Chen, M. Selbach, Global quantification of mammalian gene expression control, Nature 473 (2011) 337–342, https://doi.org/10.1038/nature10098.

[67] F. Lebrin, M.-J. Goumans, L. Jonker, R.L.C. Carvalho, G. Valdimarsdottir, M. Thorikay, C. Mummery, H.M. Arthur, P. ten Dijke, Endoglin promotes endothelial cell proliferation and TGF-beta/ALK1 signal transduction, EMBO J. 23 (2004) 4018–4028, https://doi.org/10.1038/sj.emboj.7600386.

[68] N.Y. Lee, B. Ray, T. How, G.C. Blobe, Endoglin promotes transforming growth factor beta-mediated Smad 1/5/8 signaling and inhibits endothelial cell migration through its association with GIPC, J. Biol. Chem. 283 (2008) 32527–32533, https://doi.org/10.1074/jbc.M803059200.

[69] K.W. Finnson, W.L. Parker, P. ten Dijke, M. Thorikay, A. Philip, ALK1 opposes ALK5/Smad3 signaling and expression of extracellular matrix components in human chondrocytes, J. Bone Miner. Res. 23 (2008) 896–906, https://doi.org/10.1359/jbmr.080209.

[70] M.-J. Goumans, Balancing the activation state of the endothelium via two distinct TGF-beta type I receptors, EMBO J. 21 (2002) 1743–1753, https://doi.org/10.1093/emboj/21.7.1743.

[71] C. Buccoliero, D. Consolante, F. Dituri, S. Mancarella, N. Hanafy, A. Mancinelli, P. Trerotoli, S. Leporatti, C. Pisano, G. Giannelli, A TGF-beta receptor I kinase inhibitor, galunisertib (LY2157299) inhibits hepatocellular carcinoma progression in in vivo experimental models, J. Hepatol. 64 (2016) S565, https://doi.org/10.1016/S0168-8278(16)01023-0.

[72] Y. Cao, R. Agarwal, F. Dituri, L. Lupo, P. Trerotoli, S. Mancarella, P. Winter, G. Giannelli, NGS-based transcriptome profiling reveals biomarkers for companion diagnostics of the TGF-beta; receptor blocker galunisertib in HCC, Cell Death Dis. 8 (2017) e2634, , https://doi.org/10.1038/cddis.2017.44.

[73] S. Hammad, E. Cavalcanti, J. Werle, M.L. Caruso, A. Dropmann, A. Ignazzi, M.P. Ebert, S. Dooley, G. Giannelli, Galunisertib modifies the liver fibrotic composition in the Abcb4Ko mouse model, Arch. Toxicol. 92 (2018) 2297–2309, https://doi.org/10.1007/s00204-018-2231-y.

[74] A. Masuda, T. Nakamura, M. Abe, H. Iwamoto, T. Sakaue, T. Tanaka, H. Koga, T. Torimura, Promotion of liver regeneration/anti-fibrotic effects of TGF-beta receptor kinase inhibitor galunisertib in CCl4-treated mice and the possibility for clinical application, Hepatology, 2018, p. 648A.

[75] D.S. Kuo, C. Labelle-Dumais, D.B. Gould, COL4A1 and COL4A2 mutations and disease: insights into pathogenic mechanisms and potential therapeutic targets, Hum. Mol. Genet. 21 (2012) R97–110, https://doi.org/10.1093/hmg/dds346.

[76] K. Gelse, E. Pöschl, T. Aigner, Collagens—structure, function, and biosynthesis, Adv. Drug Deliv. Rev. 55 (2003) 1531–1546, https://doi.org/10.1016/J.ADDR.2003.08.002.

[77] J. Guo, H. Yao, X. Lin, H. Xu, D. Dean, Z. Zhu, G. Liu, P. Sime, IL-13 induces YY1 through the AKT pathway in lung fibroblasts, PLoS One 10 (2015) 1–17, https://doi.org/10.1371/journal.pone.0119039.